NSWCDD/TR-92/237

NONLINEAR RESISTIVE GRID WAVELET TRANSFORMATIONS FOR TEXTURE FEATURE EXTRACTION

BY GEORGE W. ROGERS CAREY E. PRIEBE
JEFFREY L. SOLKA
STRATEGIC SYSTEMS DEPARTMENT

JUNE 1992

NAVAL SURFACE WARFARE CENTER
DAHLGREN DIVISION
Dahlgren, Virginia 22448-5000

NSWCDD/TR-92/237

NONLINEAR RESISTIVE GRID WAVELET TRANSFORMATIONS FOR TEXTURE FEATURE EXTRACTION

BY GEORGE W. ROGERS CAREY E. PRIEBE
JEFFREY L. SOLKA
STRATEGIC SYSTEMS DEPARTMENT

JUNE 1992

NAVAL SURFACE WARFARE CENTER
DAHLGREN DIVISION
Dahlgren, Virginia 22448-5000

FOREWORD

Target identification using gray-scale texture information is of interest both to the surveillance and interceptor design communities. This report details an analog scheme to extract texture features to use for target discrimination. The features extracted from this system could be used either as part of an alert system for a human surveillance team or as part of a terminal homing seeker in an autonomous kill vehicle.

This work has been supported by a number of sponsors and has been conducted in the Space and Ocean Geodesy Branch.

This report has been reviewed by Dr. Richard A. Lorey, Head of the Space and Ocean Geodesy Branch and James Sloop, Head of the Space and Surface Systems Division.

Approved by:

R. L. SCHMIDT, Head
Strategic Systems Department

ABSTRACT

This report describes an analog method to extract gray-scale texture features. This method uses a nonlinear resistive grid to perform a two-dimensional pseudowavelet transform of the initial input image. Texture features are computed using first- and second- order variance estimates of the transform coefficients. Some preliminary results are presented indicating the natural segmentation that the nonlinearity provides at the boundary of two dissimilar textures.

CONTENTS

ILLUSTRATIONS

FIGURES (CONTINUED)

INTRODUCTION

The silicon retina of Mead[1] displays many features of human retinal processing. The key feature of interest here is the center-surround response of each node in the retina that is reminiscent of a mother wavelet.[2] This center-surround response is accomplished by differencing the input at a pixel with a local average computed via an analog resistive grid. In this report, we focus on the utility of these analog pseudowavelet coefficients. We include an example where the multiresolution wavelet coefficients have been further processed to produce local variance and variance of variance features that can be used to perform texture discrimination. The full details of the hybrid optoelectronic implementation of this system are addressed elsewhere.[3] The twin advantages of this hybrid approach are the near real-time processing to obtain wavelet coefficients and/or texture features and the nonlinear, data-driven nature of the effective wavelets produced by a resistive grid composed of nonlinear components.

BACKGROUND

As an outgrowth of previous work in texture discrimination based on fractal dimension derived power law features,[4, 5] we have recently started to consider using a (hypothetical) silicon retina to do image preprocessing for texture analysis. There are twin motivations for this line of investigation. First and foremost, the texture discrimination ability of retinal-based biological systems provides a working prototype for this approach.

Second, an analog implementation of our hypothetical retina offers the potential of real-time preprocessing. The postprocessing is based on well understood parametric and nonparametric statistical techniques.[6] This permits an analysis of the contributions of individual features produced in the preprocessing and gives us a capability to follow an *evolutionary* or experimental approach with our silicon retina model. We can delete features that do not perform, while trying variations on new or good features. Central to our model is the set of nonlinearities encountered in analog very large scale integrated (VLSI) implementations as well as in biological systems. These nonlinearities are crucial, for example, to both segmentation and the prevention of feature contamination between disparate texture types.

Our (hypothetical) silicon retina is centered on the use of two-dimensional resistive grids. A resistive grid functions to smooth the input in a linear or (of interest to us) a nonlinear fashion. In its linear version, the resistive grid smoothes the inputs to produce an output that corresponds approximately to the convolution of the input image with an exponential kernel with a characteristic length or kernel size we will denote by L_k or, equivalently, by an associated scale ϵ_k.

Let $f:\mathbb{R}^2 \rightarrow \mathbb{R}$ be the function that produces our two-dimensional input image defined on a discrete (pixel) array. Further, let $R_\varepsilon(f):\mathbb{R}^2 \times \mathbb{R} \rightarrow \mathbb{R}^2 \times \mathbb{R}$ be the resistive grid transform of f at scale ε. Suppose that we compute $R_\varepsilon(f)$ for n different scales: $R_2^0(f), R_2^1(f), R_2^2(f),..., R_2^{n-1}(f)$. Notationally, we let $L_\beta = R_2^{\beta-1}(f)$. The L_β can be thought of as functional estimates at different levels of smoothing. Next, we compute a set of features for each pixel:

$$F_\alpha = R_2^{\alpha-1}(f) - R_2^{\alpha}(f) = L_\alpha - L_{\alpha+1}\ ,\ \alpha=1,...,n-1.$$

We now have a set of n-1 features defined at each array or grid (pixel) point that correspond to a difference of kernels of different characteristic scales. These are the (nonlinear) resistive grid analogs of the difference-of-Gaussian wavelet basis. Thus, at each pixel, we have the first n-1 coefficients of a wavelet (or pseudowavelet) basis with the F_α being the coefficient arrays.

Ganglion cells in the retina of the cat are of two types, those that respond to hyperpolarizing signals, and those that respond to depolarizing signals.[7] Each type performs a half-wave rectification operation on the signal it receives. Carver Mead has demonstrated the feasibility of performing half- and full-wave rectification in analog VLSI. Therefore, it makes sense to produce features based on this physiological structure and analog VLSI capability.

An obvious feature to compute using the twin elements of resistive grids and full-wave rectifiers is a mean variance of the pseudowavelet coefficients as a function of scale. The goal is to compute features that are relatively texture invariant. We compute these variance features v_α as follows:

$$v_\alpha = R_2^{\alpha+\tau}(|F_\alpha - R_2^{\alpha}(F_\alpha)|)$$

Here, $\tau \in \{1,2,...\}$ is chosen to smooth these variance estimates–essentially, this last smoothing is analogous to basebanding on some carrier frequency.

This gives a set of additional features for each array location (pixel) that give a measure of the variance of the difference of kernel features for the different scales. This set of steps can be repeated (iterated) using v_k as input (instead of F_k) to produce a set of second order variances v_{kk}. Thus, we have a truncated double expansion in pseudowavelet coefficients and orders of variance of these coefficients for each array location or pixel.

RESULTS

In this section, a discussion of the linear version of our functional estimation technique is given along with some nonlinear simulation results. A full analytical treatment of the nonlinear theory is beyond the scope of this report. For analytical purposes, consider a linear approximation to our functional estimation technique. Call the exponential function $\phi(x)$ (see Figure 1*), obtained from the resistive grid, which is our scaling function. We then have, as our *mother wavelet* $\psi(x)$, the difference of exponentials depicted in Figure 2. Figure 3 gives $\psi(x)$ at three different scale values. The effect of the nonlinearity of the (simulated) analog VLSI implementation on this wavelet is depicted in Figures 4a and 4b. Figure 4a shows the discontinuous input, while Figure 4b compares the $\psi(x)$ function corresponding to the linear case and the nonlinear theory. The effect of this *adaptive* wavelet amounts to a segmentation effect in the case where there is a sharp discontinuity (an edge) in the input such as in Figure 4a. That these nonlinear effects allow for an automatic segmentation can be seen from the ability of the resistive grid kernel estimator (RFKE) to model discontinuities in probability density functions while maintaining an otherwise smooth estimate (see Figures 5 and 6, reproduced from Reference 8). The resistive elements in the nonlinear resistive grid have variable conductance values. By producing a conductance map of the resistive grid, a natural segmentation occurs as can be seen in Figures 7b and 8b corresponding to the input images Figures 7a and 8a, respectively. The dark areas in Figures 7b and 8b correspond to drastically reduced conductance values. These reduced conductance values serve to greatly limit the contribution of one texture type to the wavelet coefficients centered in an adjacent texture type, which is exactly the effect seen in Figure 4b.

For the one-dimensional example input of Figure 9 (a vertical slice down the center, i.e., bushes to turret to tread to grass, of the image depicted in Figure 7a), this produces the functional approximations $L_j(x)$ (Figure 9), and differencing L_j and L_{j-1} will yield terms $F_j(x)$ analogous to the *wavelet coefficients* (Figure 10). Considering the deviations of $F_j(x)$ from a smoothed *regression* $v_j(x)$ of $F_j(x)$ (Figure 11), and the deviations of $v_j(x)$ from a smoothed *regression* $v_{kk}(x)$ of $v_j(x)$ (Figure 12), as features indicative of texture, preliminary discriminant analysis indicates encouraging capabilities to distinguish the different classes of texture.

Figure 13 depicts the high degree of separation between the three classes (grass, bush, and tank) found in Figure 7a in a derived feature space based on these resistive grid wavelet transformation features. Figures 14 and 15 similarly indicate very good discriminant capability for five classes (grass, trees, field, road, and building) found in Figure 8a. Nonparametric discriminant analysis results already show a marked improvement over results that have been obtained using traditional power law features, and the nonlinear segmentation effects appear to be central to these results. Feature analysis has shown that the first- and second-order variance features are of equal relative importance in the texture discrimination.

To illustrate the full power of our approach, one more example will be discussed. Figure 16 is a 255 gray-level *texture quilt* consisting of 16 different textures. A similar image has appeared previously in the literature in conjunction with the unsupervised texture discrimination

* All figures are included after the References.

work of Jain and Farrokhnia.[9] Each patch is 128 x 128 pixels for a total size of 512 x 512. Figure 17 shows the degree of separation obtained for the 16 classes in a derived feature space. Each class is represented by 250 points randomly chosen in a 100 x 100 square positioned so its center is coincident with the center of the patch. As can be seen from Figure 17, a high degree of separability exists for most of the classes. It should also be emphasized that those classes overlapping in this projection can be separated in some of the other three-dimensional derived feature spaces.

CONCLUSION

Our approach seems to be a powerful tool in identifying features useful in texture representation for (one type of) machine vision. In doing a comparison with biological retinas, we are several steps behind the ganglia layer. Thus, we are in some sense trying to find our way from the retinal preprocessing backwards toward the higher processing levels. In finding what works in the analog realm, it is hoped we will shed some light on the biological realm as well.

An electronic design for near real-time processing has been presented to obtain wavelet coefficients and/or texture features. Also, simulation results show that the nonlinear, data-driven character of the wavelets obtained from nonlinear resistive grids can be an advantage rather than a disadvantage, especially where a high contrast boundary separates different textures. The conversion of the wavelet coefficient maps to local power or variance features has been demonstrated to yield a useful set of features for texture discrimination.

Future work will address the need for comparison with more conventional wavelet techniques, including an analysis of the nonlinear character of the wavelet response.

REFERENCES

1. Mead, C., *Analog VLSI and Neural Systems*, Addison-Wesley, 1989.

2. Mallat, S.G., "A Theory for Multiresolution Signal Decomposition: The Wavelet Representation," *IEEE Trans. Pattern Anal. & Mach. Intell.*, Vol. 11, pp. 674-693, 1989.

3. Rogers, G. W.; Solka, J. L.; Priebe, C. R.; and Szu, H., "Opto-Electronic Computation of Wavelet-like Based Features," submitted to *Optical Engineering*, 1992.

4. Solka, J.L.; Priebe, C.E.; and Rogers, G.W., (1992),"An Initial Assessment of Discriminant Surface Complexity for Power Law Features," *Simulation*, Vol. 58, pp 311-318, 1992..

5. Priebe, C.E.; Solka, J.L.; Ellis, J.B.; and Rogers, G.W., "On Discriminant Surface Complexity for Power Law Features," submitted to *Pattern Recognition*, 1992.

6. Priebe, C.E. and Marchette, D.J., "Adaptive Mixtures: Recursive Nonparametric Pattern Recognition," *Pattern Recognition*, Vol. 24, pp. 1197-1209, 1991.

7. Spillmann, L. and Werner, J. Eds., "Visual Perception The Neurophysiological Foundations," Academic Press, 1990.

8. Poston, W.; Rogers, G.W.; Priebe, C.E.; and Solka, J.L., "Resistive Grid Kernel Estimator," submitted to *Pattern Recognition Letters*, 1992.

9. Jain, A.K. and Farrokhnia, F., "Unsupervised Texture Segmentation Using Gabor Filters," *Pattern Recognition*, Vol. 24, pp. 1167-1186, 1991.

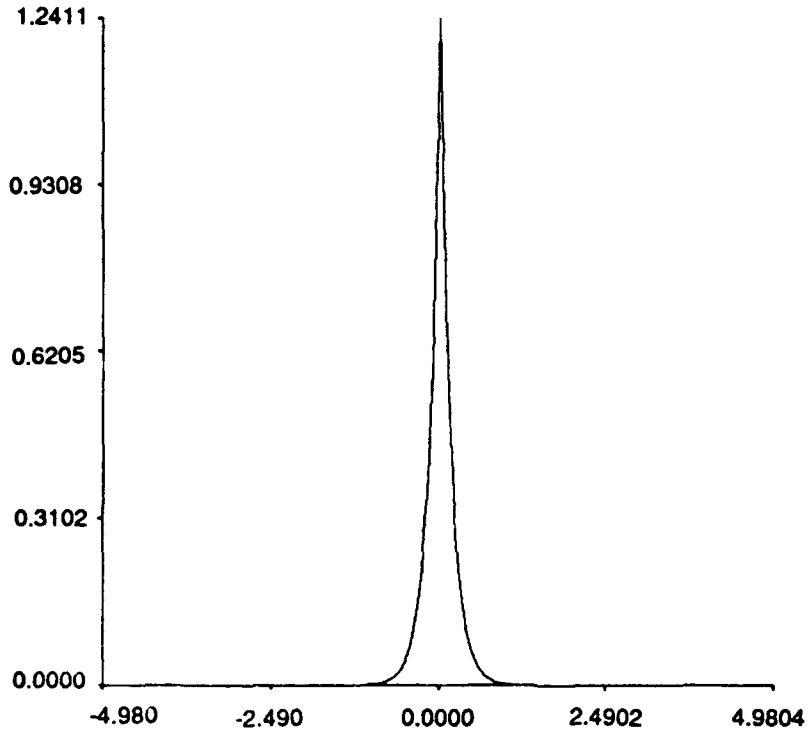

FIGURE 1. SCALING FUNCTION FOR ONE-DIMENSIONAL RESISTIVE GRID WITH LINEAR COMPONENTS

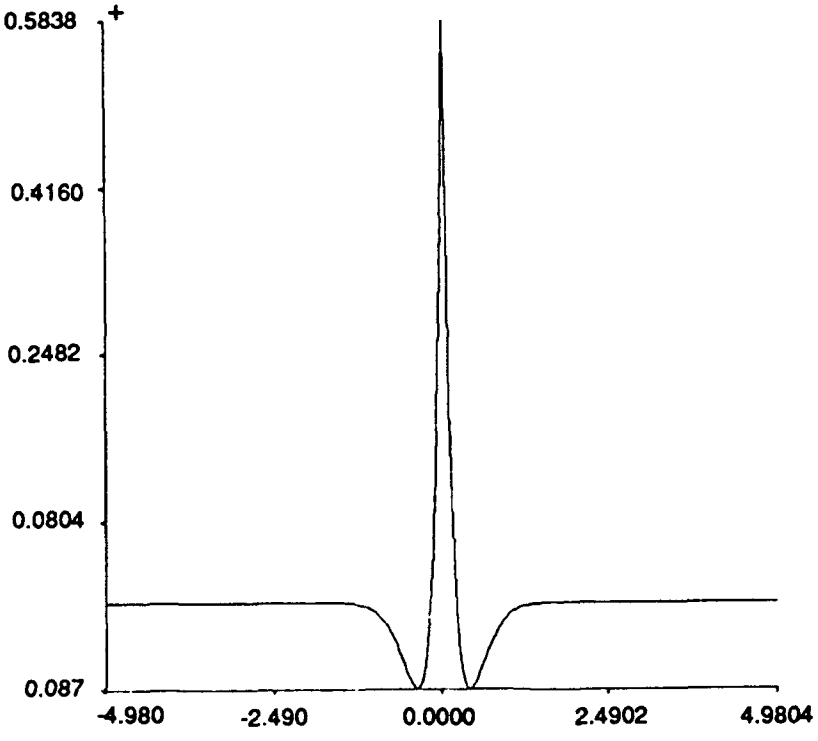

FIGURE 2. MOTHER WAVELET $\psi(x)$ FOR ONE-DIMENSIONAL RESISTIVE GRID WITH LINEAR COMPONENTS

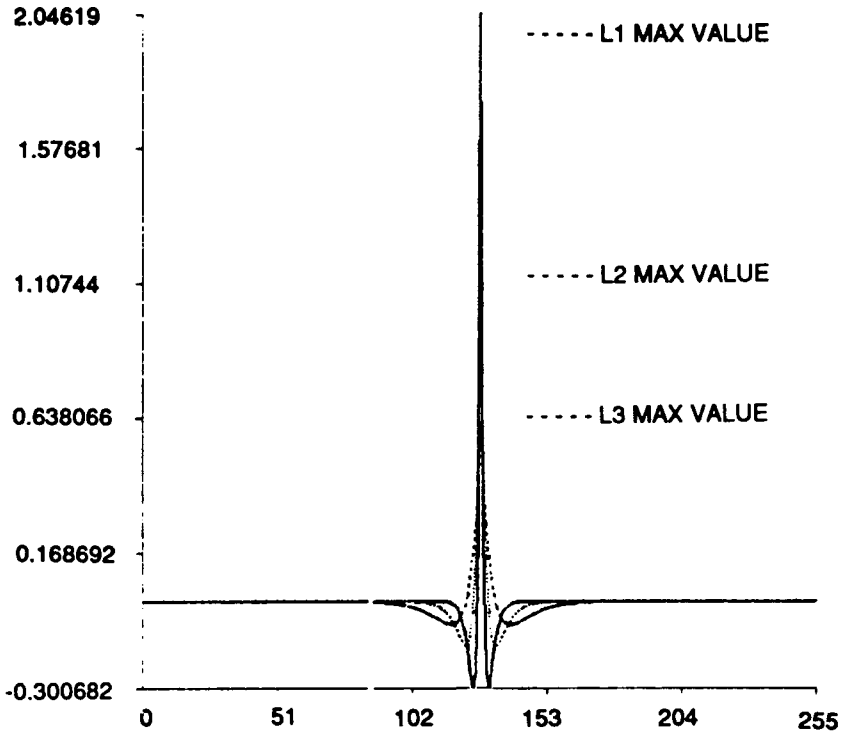

FIGURE 3. ONE-DIMENSIONAL RESISTIVE GRID WAVELETS AT THREE INCREASING SCALES

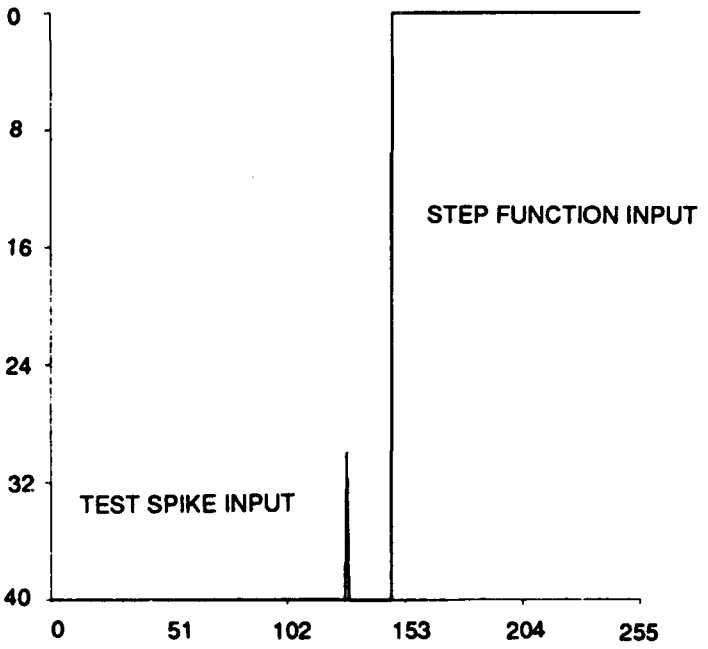

Note: The grid is allowed to come to equilibrium with the step function input; then resistances are held fixed while the spike is input. See Figure 4b for the effective resultant wavelet for the spike component of the total input.

FIGURE 4A. NONLINEAR ONE-DIMENSIONAL RESISTIVE GRID INPUT

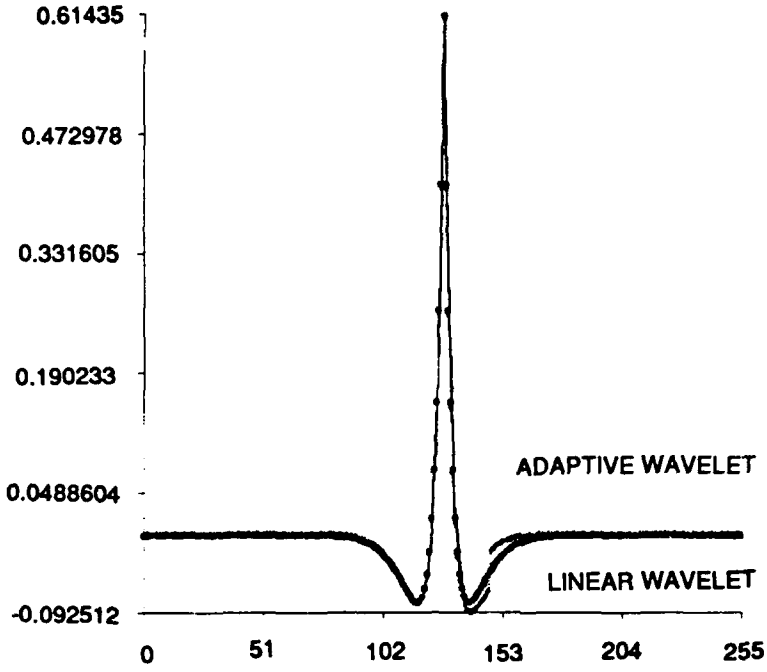

Note: The nonlinear response strongly damps the wavelet amplitude at a contrast boundary.

FIGURE 4B. EFFECTIVE RESULTANT LINEAR AND NONLINEAR WAVELET FOR SPIKE COMPONENT OF TOTAL INPUT SHOWN IN FIGURE 4A

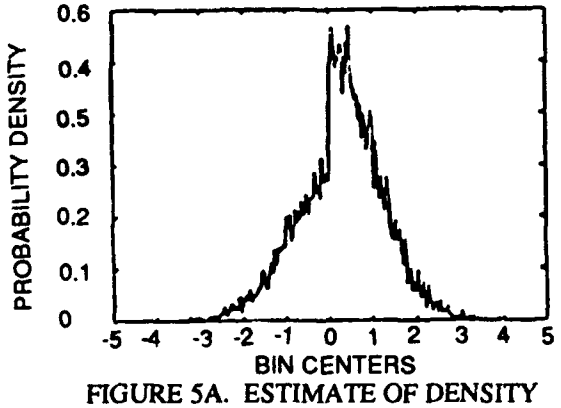

FIGURE 5A. ESTIMATE OF DENSITY USING HISTOGRAM

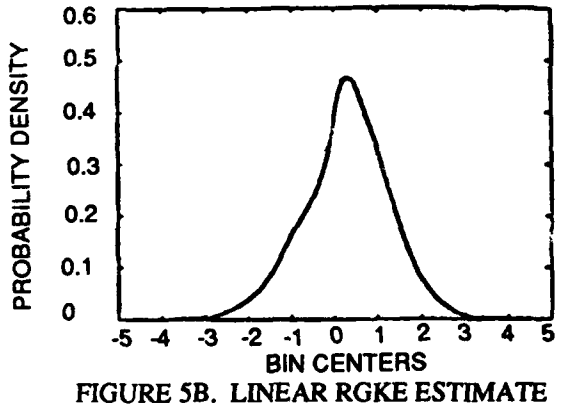

FIGURE 5B. LINEAR RGKE ESTIMATE WITH L=5.0

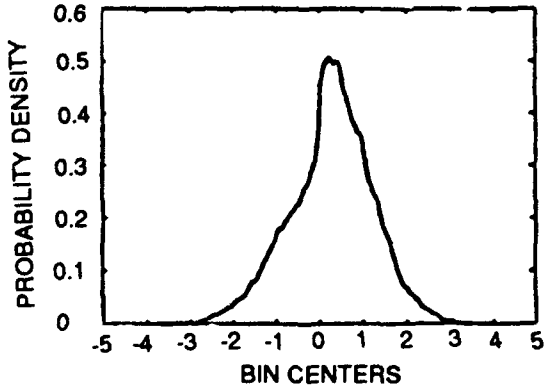

FIGURE 5C. LINEAR RGKE ESTIMATE WITH L=2.0

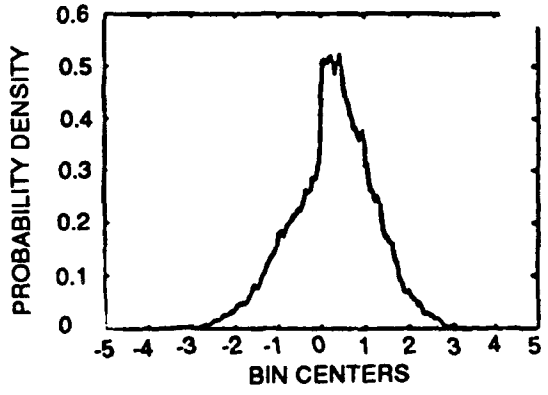

FIGURE 5D. LINEAR RGKE ESTIMATE WITH L=1.0

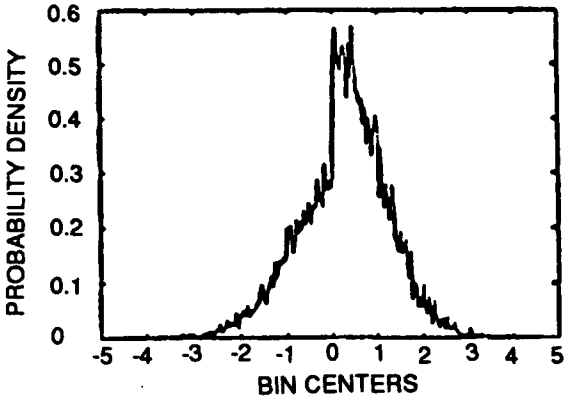

FIGURE 6A. ESTIMATE OF DENSITY USING HISTOGRAM

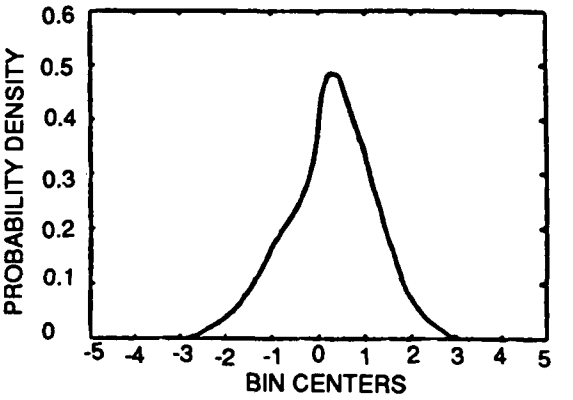

FIGURE 6B. NONLINEAR RGKE ESTIMATE WITH β=0.2

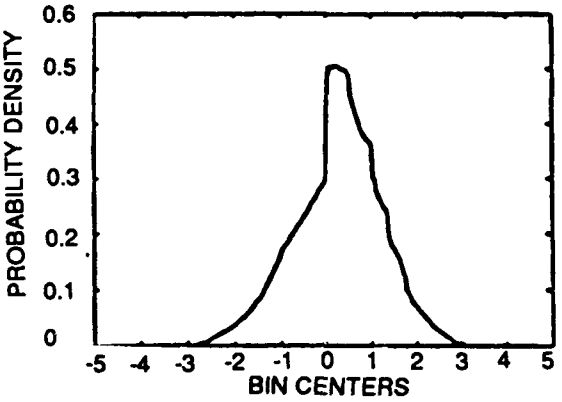

FIGURE 6C. NONLINEAR RGKE ESTIMATE WITH β=1.0

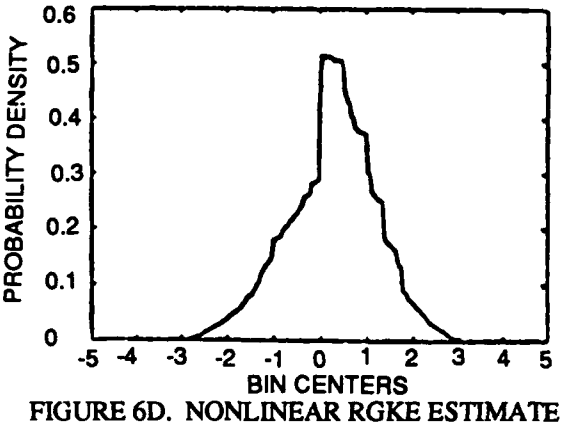

FIGURE 6D. NONLINEAR RGKE ESTIMATE WITH β=2.0

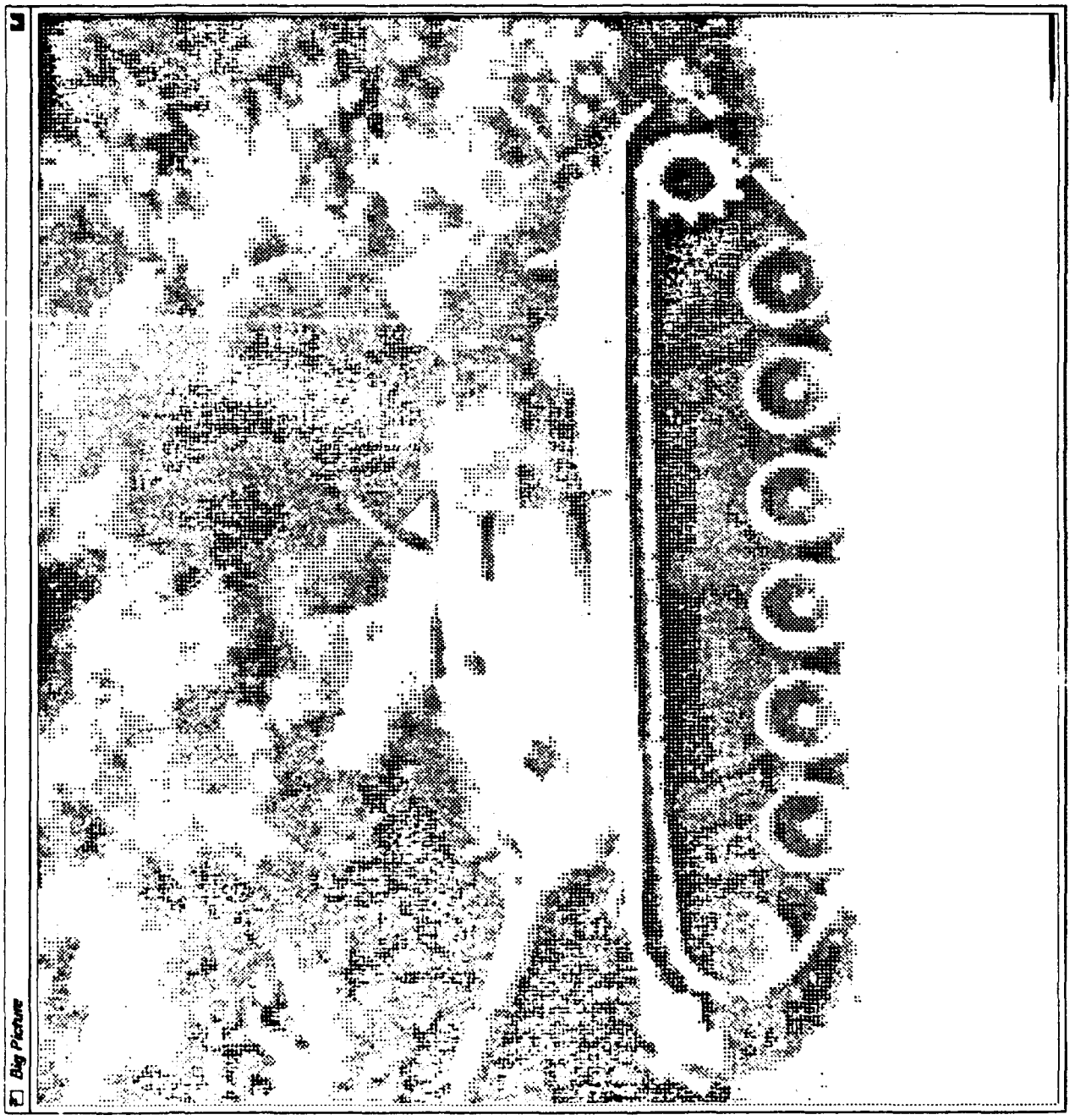

FIGURE 7A. TANK IMAGE INPUT TO NONLINEAR TWO-DIMENSIONAL RESISTIVE GRID

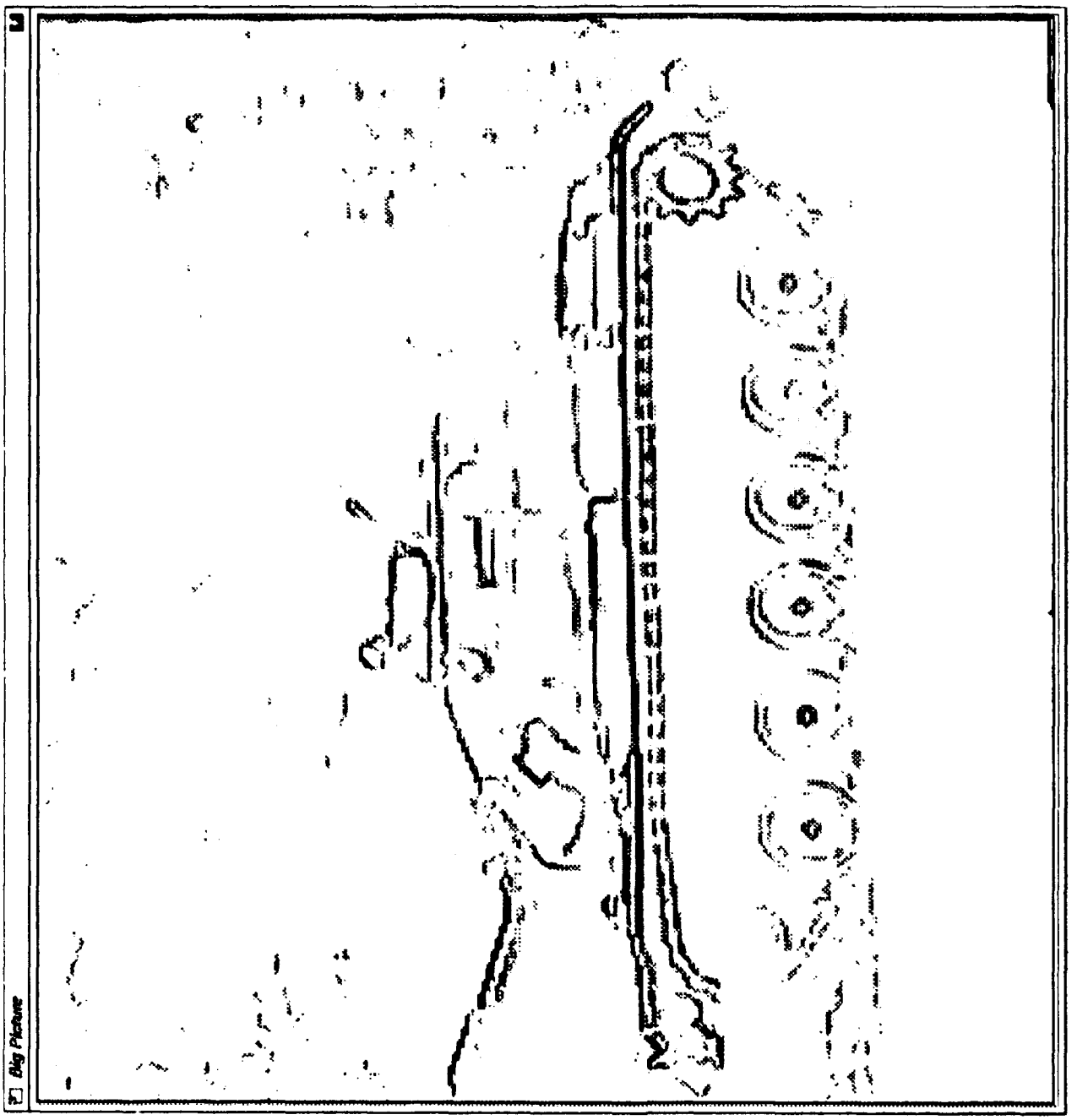

NOTE: The conductance map has performed segmentation at all of the higher contrast boundaries.

FIGURE 7B. RESULTANT CONDUCTANCE MAP FOR TANK IMAGE FOR MODERATE NONLINEARITY SETTING

FIGURE 8A. AERIAL IMAGE INPUT TO NONLINEAR TWO-DIMENSIONAL RESISTIVE GRID

Note: The conductance map has performed segmentation at all of the higher contrast boundaries. The highest contrast boundaries are typically due to man-made structures.

FIGURE 8B. RESULTANT CONDUCTANCE MAP FOR AERIAL IMAGE FOR MODERATE NONLINEARLITY SETTING

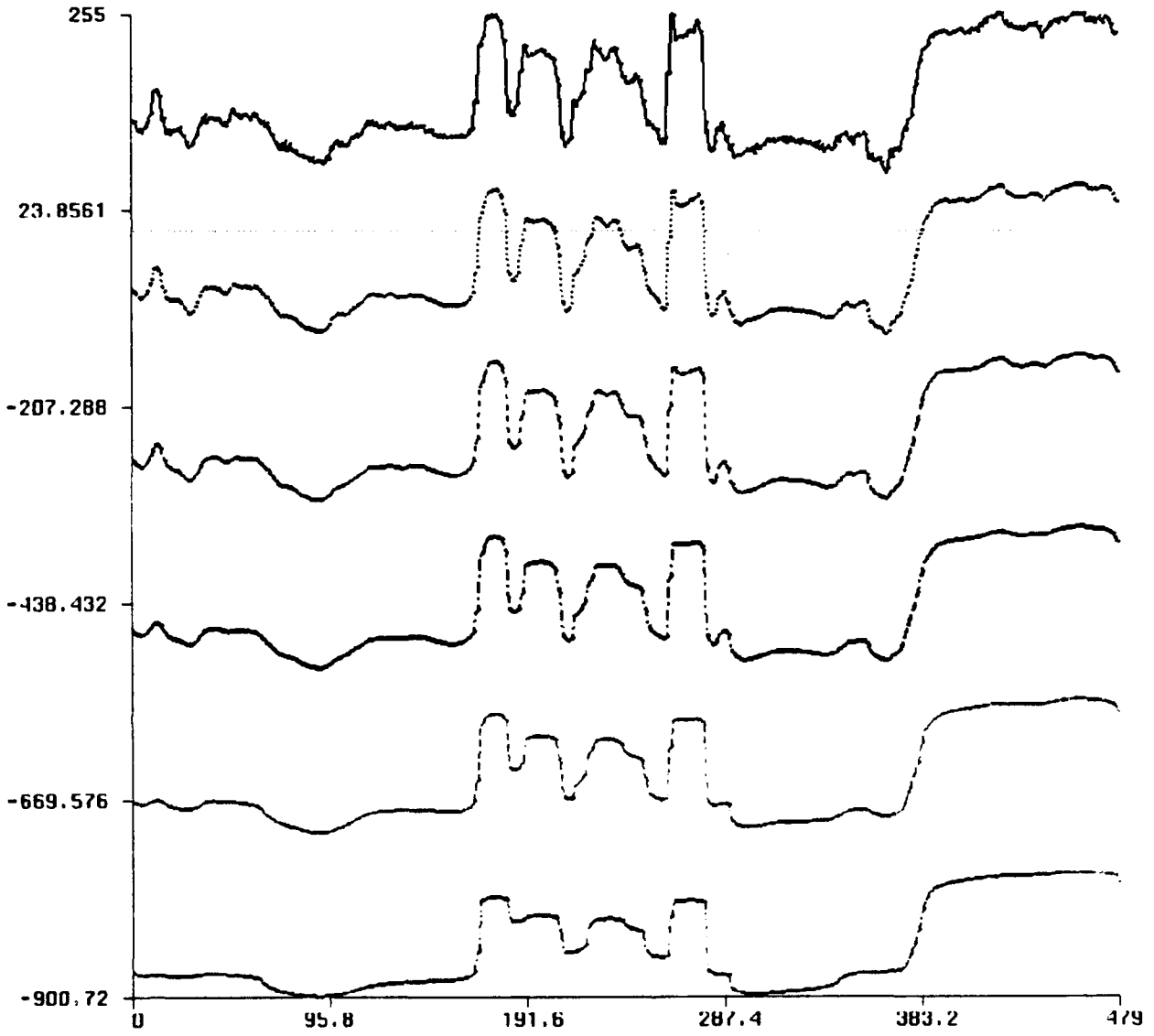

Note: Each output has been offset vertically for clarity.

FIGURE 9. TOP TO BOTTOM: ONE-DIMENSIONAL INPUT (TOP LINE) PRODUCED BY TAKING VERTICAL (TURRET TO TREAD) SLICE OF TANK IMAGE OF FIGURE 7A; RESISTIVE GRID OUTPUTS AT SUCCESSIVELY DOUBLED SCALES

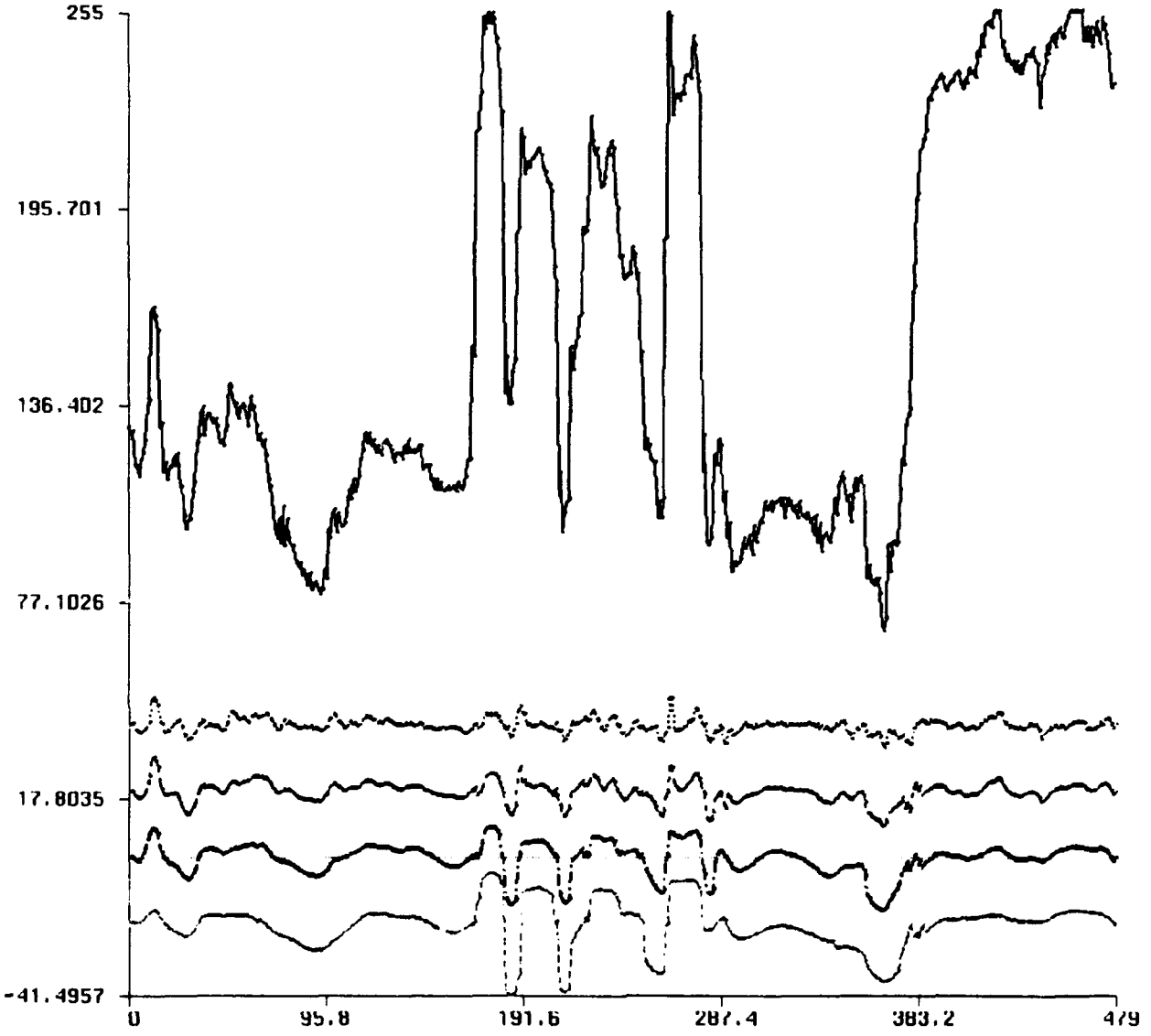

Note: Each output has been offset vertically for clarity. The input (top line) is the same as for Figure 9.

FIGURE 10. TOP TO BOTTOM: ONE-DIMENSIONAL INPUT (TOP LINE) PRODUCED BY TAKING VERTICAL (TURRET TO TREAD) SLICE OF TANK IMAGE OF FIGURE 7A; SUCCESSIVE WAVELET COEFFICIENTS

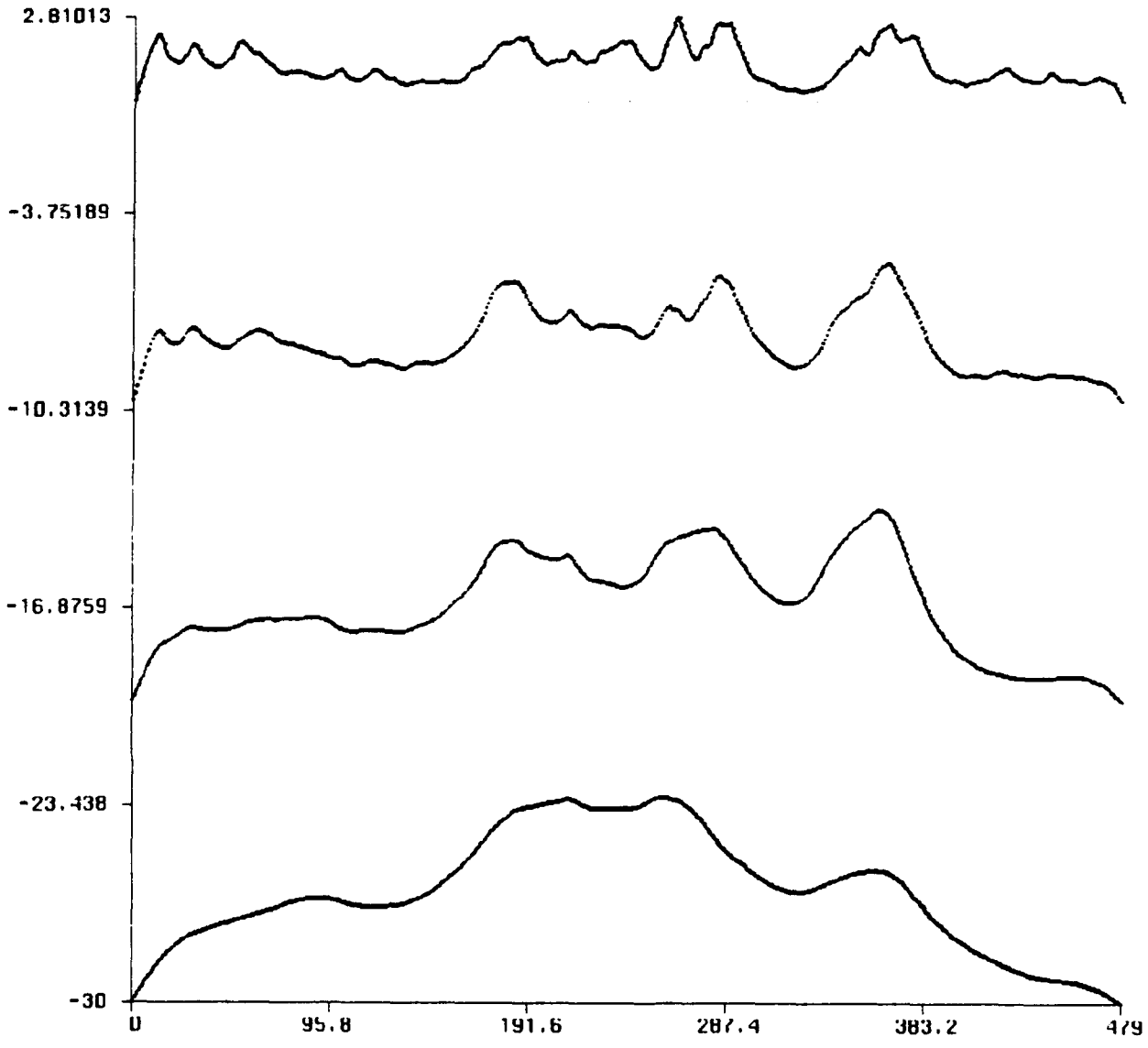

Note: Each output has been offset vertically for clarity.

FIGURE 11. TOP TO BOTTOM: ANALOG REGRESSION COEFFICIENTS FOR INCREASING SCALE

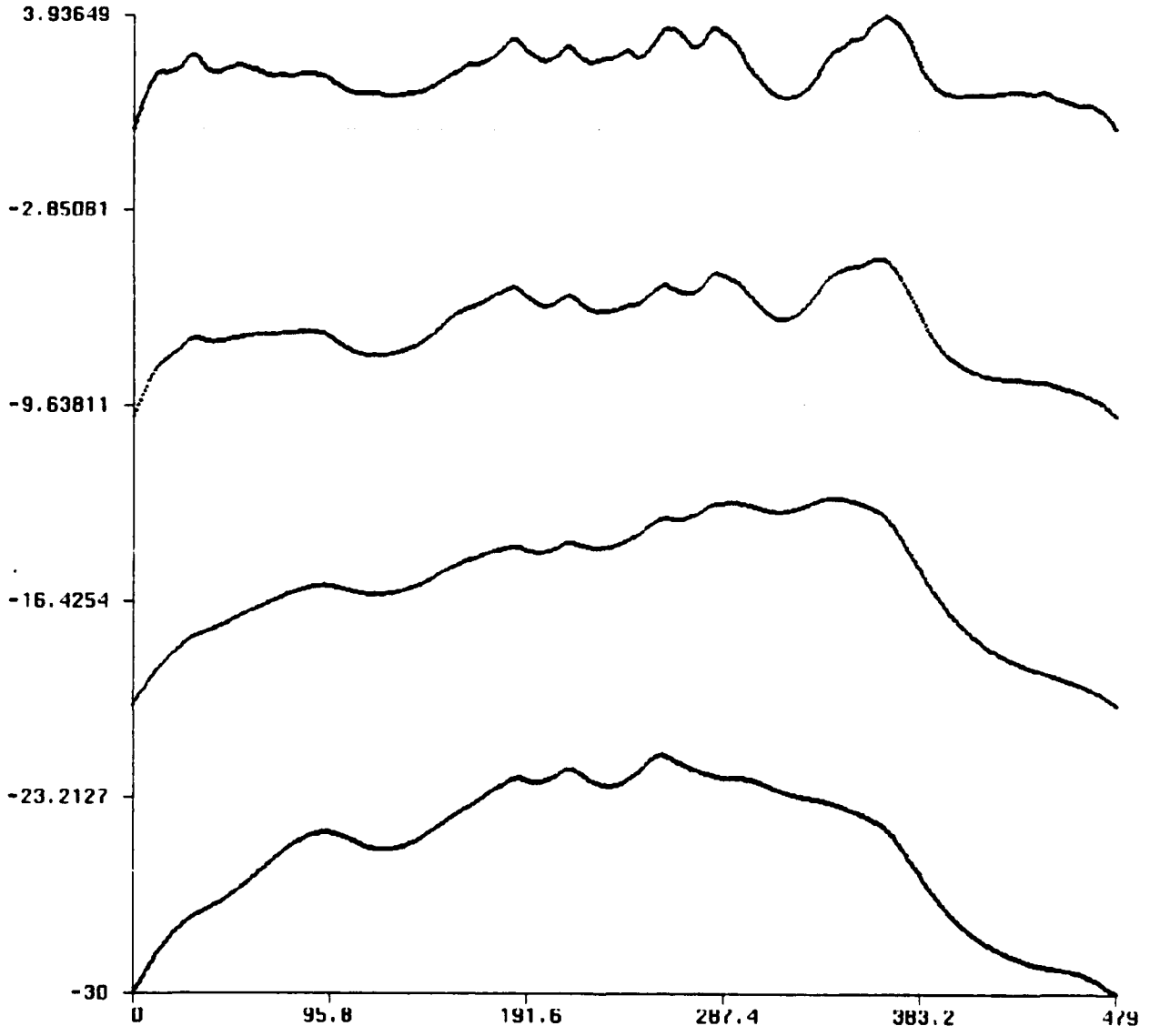

Note: Each output has been offset vertically for clarity.

FIGURE 12. TOP TO BOTTOM: SECOND-ORDER ANALOG REGRESSION COEFFICIENTS FOR INCREASING SCALE

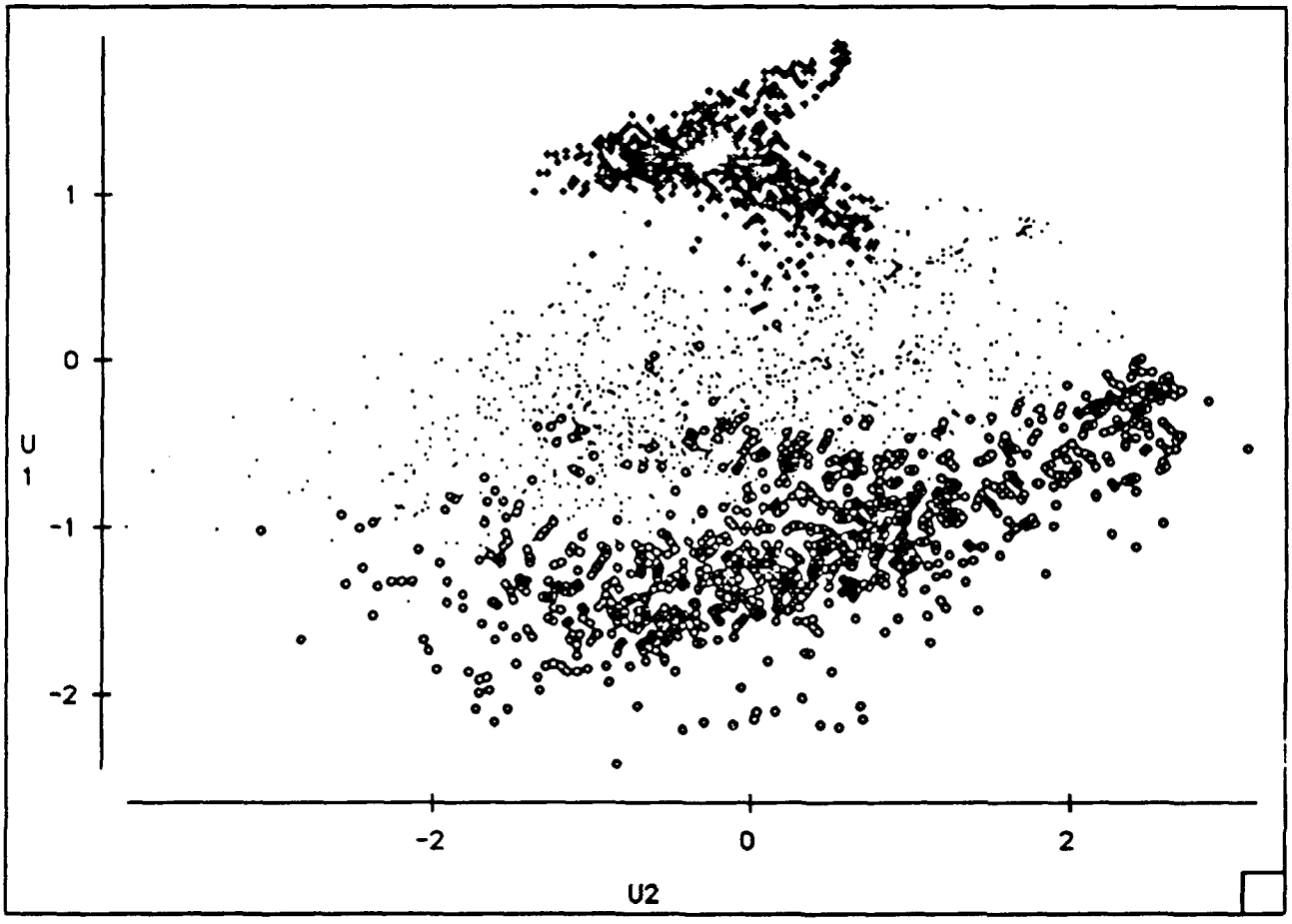

Legend: + Grass
. Bush
o Tank

Note: U1 vs. U2 (first two principal components)
1000 observations per class

FIGURE 13. THREE-CLASS SCATTER PLOT OF DERIVED RESISTIVE GRID WAVELET TRANSFORMATION (RGWT) DATA

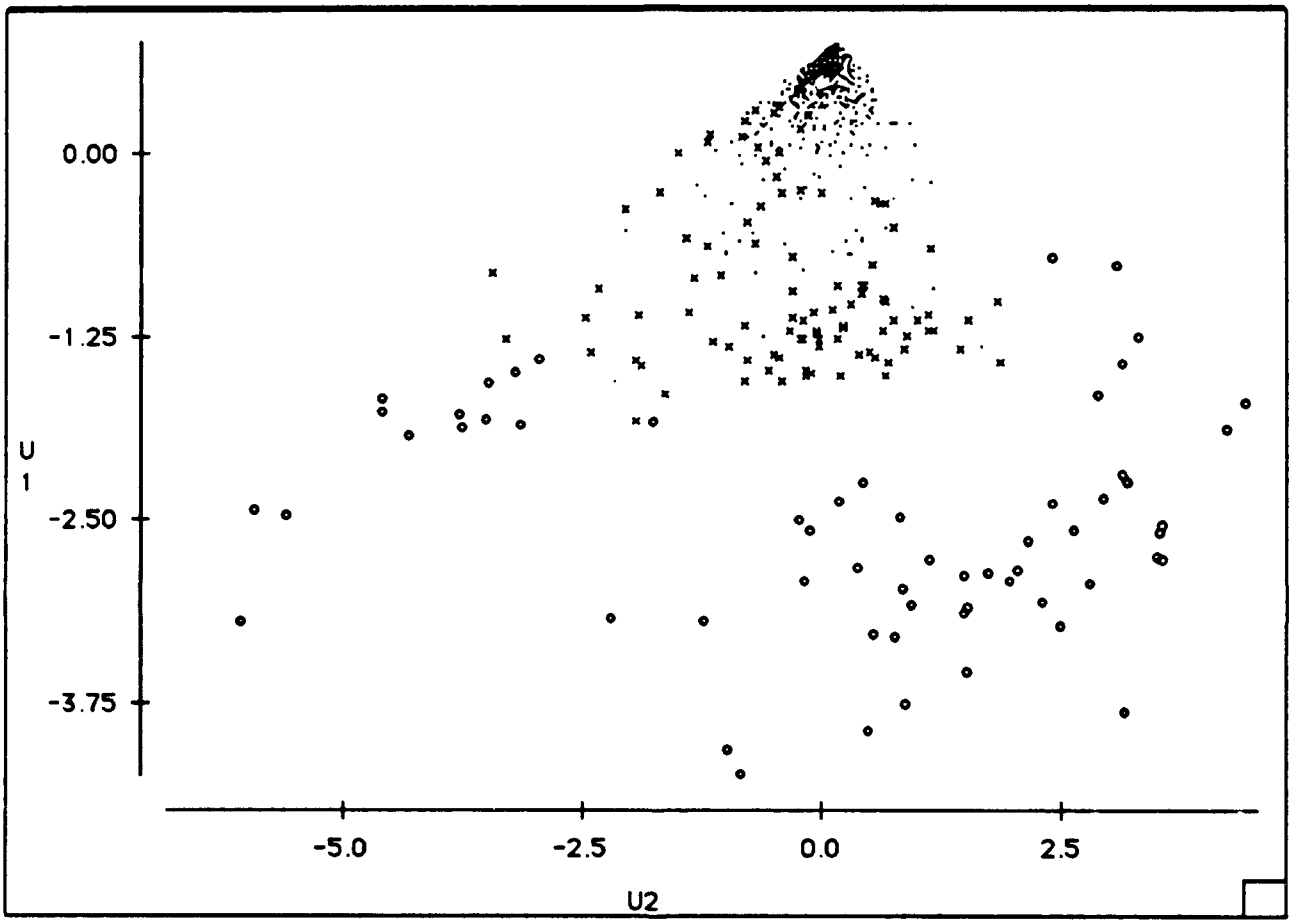

Legend: o Building
x Road
. Grass, Trees, Field

Note: U1 vs. U2 (first two principal components)
1000 observations per class

FIGURE 14. BUILDINGS VS. ROAD IN RGWT FEATURE SPACE

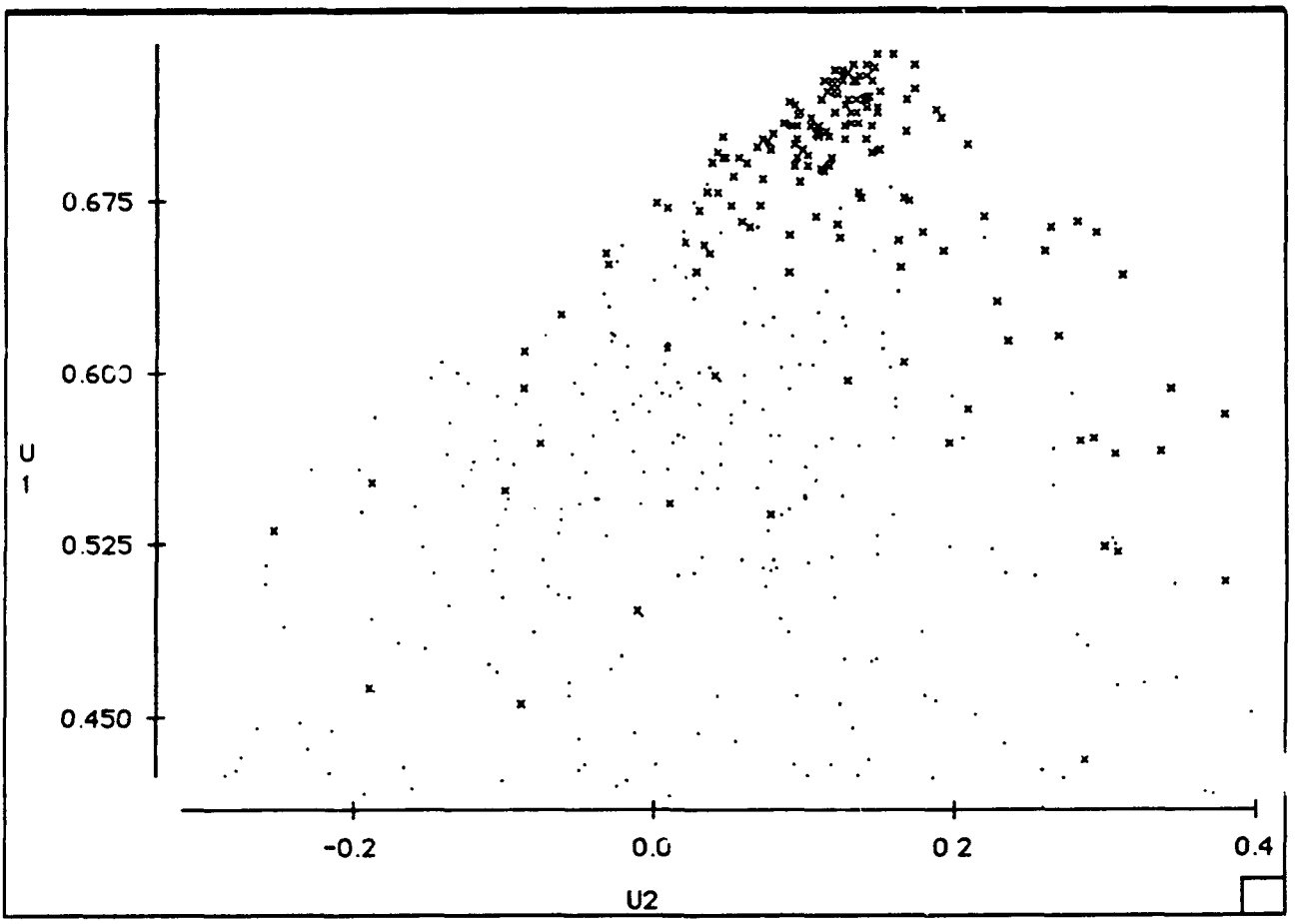

Legend: x Field
Grass, Trees, Building, Road

Note: U1 vs. U2 (first two principal components)
1000 observations per class

FIGURE 15. FIELDS VS. OTHER IN RGWT FEATURE SPACE

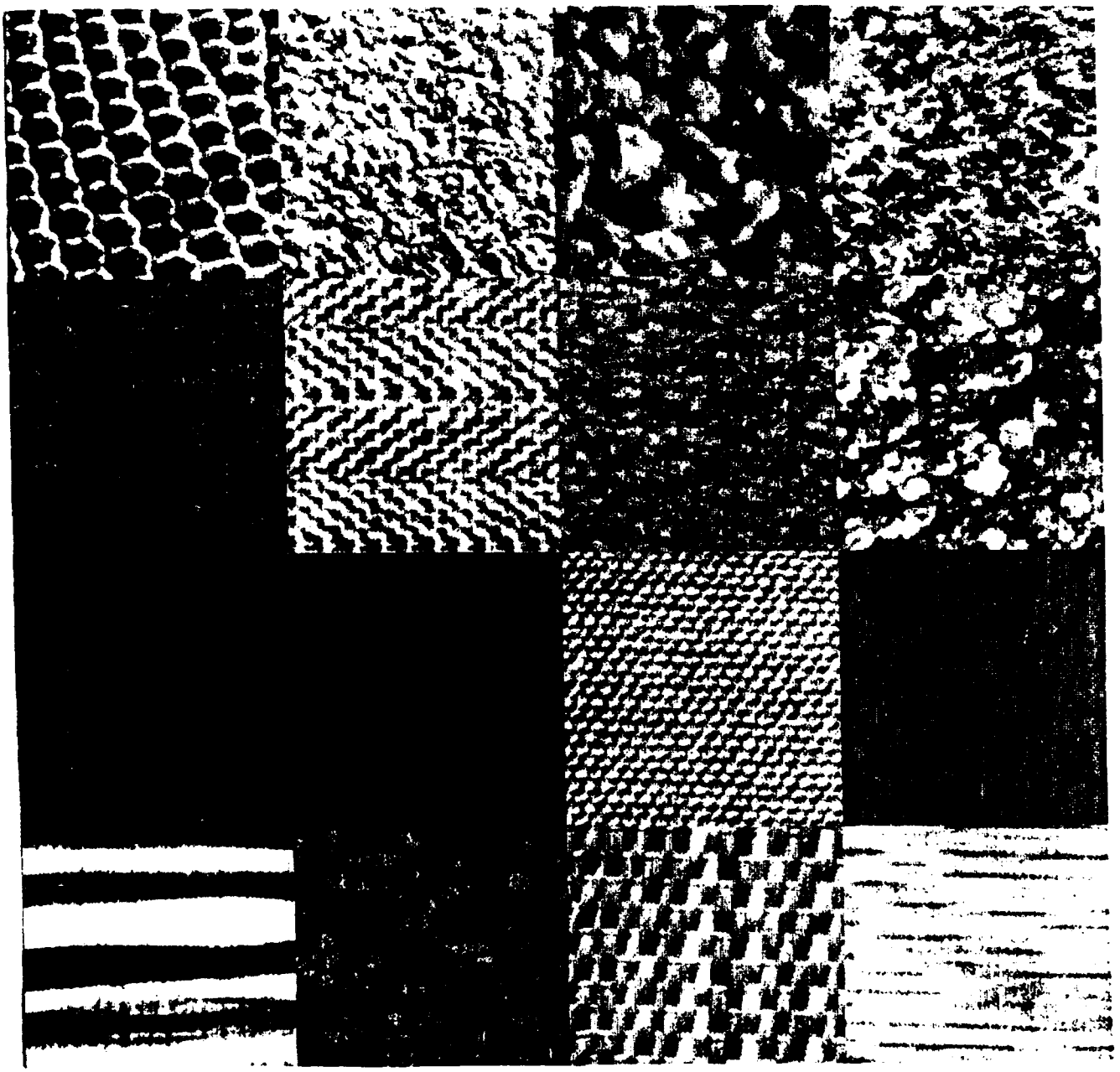

FIGURE 16. 16-PATCH TEXTURE QUILT

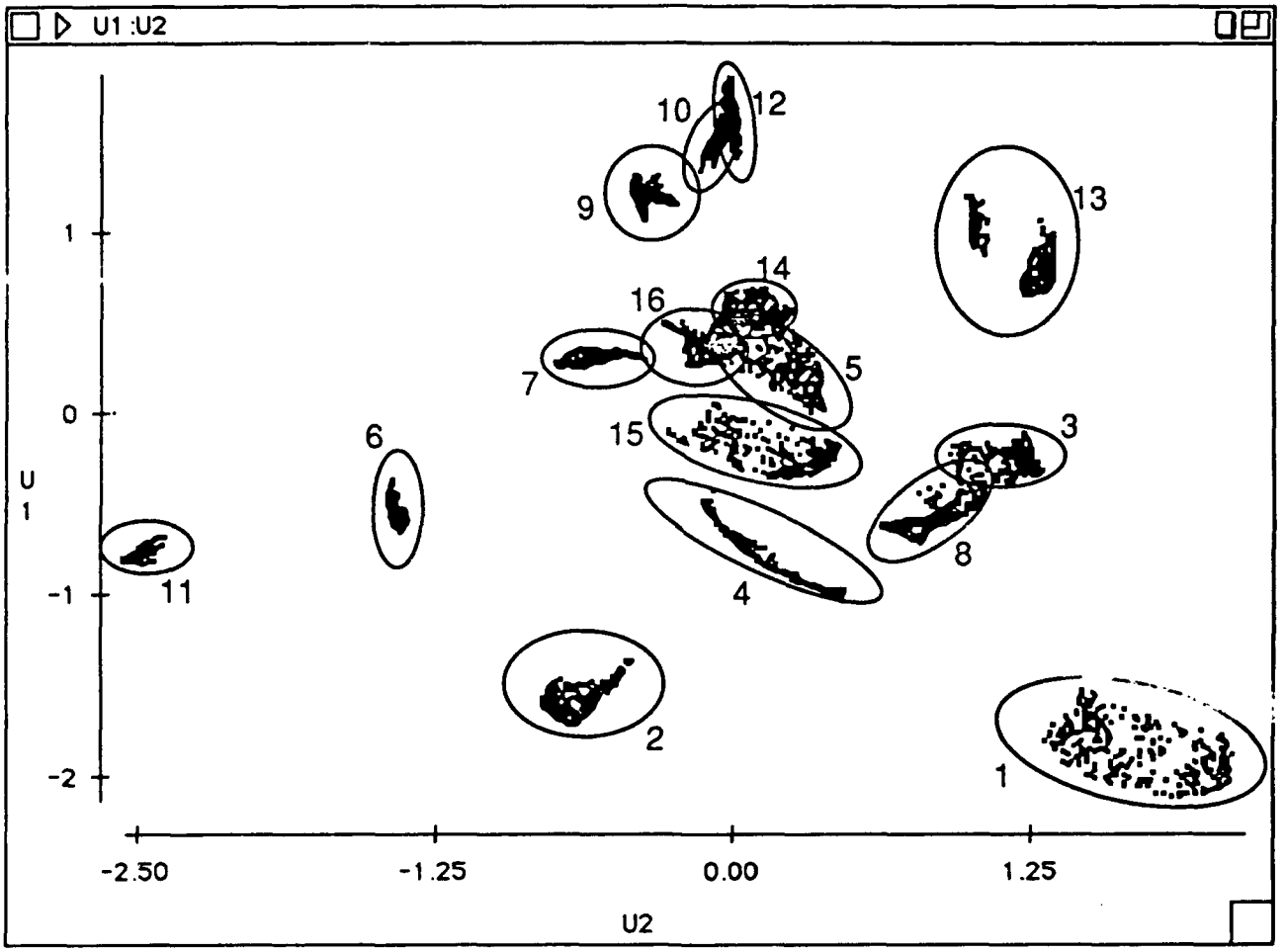

Note: Numbering has been done consecutively top to bottom across the rows.

FIGURE 17. SEPARATION OF 16 QUILT PATCHES IN DERIVED FEATURE SPACE

DISTRIBUTION

	COPIES
ATTN CODE 213 SIEGEL OFFICE OF NAVAL TECHNOLOGY 800 N QUINCY ST ARLINGTON VA 22217-5000	1
ATTN THOMAS MCKENNA HAROLD HAWKINS OFFICE OF CHIEF OF NAVAL RESEARCH COGNITIVE AND NEURAL SCIENCE DIV 800 N QUINCY ST ARLINGTON VA 22217-5000	1 1
ATTN CLIFFORD LAU OFFICE OF CHIEF OF NAVAL RESEARCH ELECTRONICS DIV 800 N QUINCY ST ARLINGTON VA 22217-5000	1
ATTN DSO YOUN DEFENSE ADVANCED RESEARCH PROJECTS AGENCY 1400 WILSON BLVD ROSLYN VA 22201	1
ATTN PAUL WERBOS NATIONAL SCIENCE FOUNDATION ROOM 1151 WASHINGTON DC 20550	1
ATTN AL GORDON 013 COMMANDER NAVAL OCEAN SYSTEMS CENTER SAN DIEGO CA 92152-5000	1
ATTN ROY STREIT COMMANDER NAVAL UNDERWATER SYSTEMS CENTER NEW LONDON CT 06320	1
ATTN DAVID MARCHETTE COMMANDER NAVAL OCEAN SYSTEMS CENTER SAN DIEGO CA 92152-5000	1
ATTN JIM MAAR R51 NATIONAL SECURITY AGENCY FT MEADE MD 20755-6000	1
DEFENSE TECHNICAL INFORMATION CENTER CAMERON STATION ALEXANDRIA VA 22304-6145	2

INTERNAL DISTRIBUTION:		
C		1
D		1
D4		1
E261	FINK	1
E231		3
E232		2
E32	GIDEP	1
E42	HYNSON	1
F33	TURNER	1
F44	POWLAK	1
G11	LUCAS	1
G23	MALYEVAC	1
G32	HOLLAND	1
G42	FARSAIE	1
G42	DUMOULIN	1
G43	CAVARIS	1
H23	DRAPER	1
K		1
K10		5
K12		5
K12	ROGERS	5
K12	POSTON	5
K12	PRIEBE	5
K12	SOLKA	5
K13		1
K14		1
K44	GLASS	1

DISTRIBUTION (CONTINUED)

		COPIES
K44	REID	1
N415	MCCLINTOCK	1
N415	HARMON	1
R44	SZU	1
R44	TELFER	1
U23	BARAN	1

REPORT DOCUMENTATION PAGE

Form Approved
OBM No. 0704-0188

1. AGENCY USE ONLY *(Leave blank)*	2. REPORT DATE	3. REPORT TYPE AND DATES COVERED
	June 1992	

4. TITLE AND SUBTITLE

Nonlinear Resistive Grid Wavelet Transformations for Texture Feature Extraction

5. FUNDING NUMBERS

6. AUTHOR(S)

George W. Rogers, Carey E. Priebe, and Jeffrey L. Solka

7. PERFORMING ORGANIZATION NAME(S) AND ADDRESS(ES)

Naval Surface Warfare Center Dahlgren Division (K12)
Dahlgren, Virginia 22448-5000

8. PERFORMING ORGANIZATION REPORT NUMBER

NSWCDD/TR-92/237

9. SPONSORING/MONITORING AGENCY NAME(S) AND ADDRESS(ES)

10. SPONSORING/MONITORING AGENCY REPORT NUMBER

11. SUPPLEMENTARY NOTES

12a. DISTRIBUTION/AVAILABILITY STATEMENT

Approved for public release; distribution is unlimited.

12b. DISTRIBUTION CODE

13. ABSTRACT *(Maximum 200 words)*

This report describes an analog method to extract gray-scale texture features. This method uses a nonlinear resistive grid to perform a two-dimensional pseudowavelet transform of the initial input image. Texture features are computed using first- and second- order variance estimates of the transform coefficients. Some preliminary results are presented indicating the natural segmentation that the nonlinearity provides at the boundary of two dissimilar textures.

14. SUBJECT TERMS

Nonlinear Resistive Grid, Wavelet Transformation, Texture Feature Extraction, Two-Dimensional Pseudowavelet Transform

15. NUMBER OF PAGES

23

16. PRICE CODE

17. SECURITY CLASSIFICATION OF REPORT	18. SECURITY CLASSIFICATION OF THIS PAGE	19. SECURITY CLASSIFICATION OF ABSTRACT	20. LIMITATION OF ABSTRACT
UNCLASSIFIED	UNCLASSIFIED	UNCLASSIFIED	SAR